Crystal Structure of the Cys2 Activator-Binding Domain of Protein Kinase Cδ in Complex with Phorbol Ester

Gongyi Zhang,* Marcelo G. Kazanietz,†
Peter M. Blumberg,† and James H. Hurley*
*Laboratory of Molecular Biology
National Institute of Diabetes
  and Digestive and Kidney Diseases
National Institutes of Health
Bethesda, Maryland 20892-0580
†Molecular Mechanisms of Tumor Promotion Section
Laboratory of Cellular Carcinogenesis and
  Tumor Promotion
National Cancer Institute
Bethesda, Maryland 20892-4255

Summary

Protein kinase Cs (PKCs) are a ubiquitous family of regulatory enzymes that associate with membranes and are activated by diacylglycerol or tumor-promoting agonists such as phorbol esters. The structure of the second activator-binding domain of PKCδ has been determined in complex with phorbol 13-acetate, which binds in a groove between two pulled-apart β strands at the tip of the domain. The C3, C4, and C20 phorbol oxygens form hydrogen bonds with main-chain groups whose orientation is controlled by a set of highly conserved residues. Phorbol binding caps the groove and forms a contiguous hydrophobic surface covering one-third of the domain, explaining how the activator promotes insertion of PKC into membranes.

Introduction

Protein kinase C (PKC) denotes a family of isozymes that play a central role in signal transduction in eukaryotes (Kikkawa et al., 1989; Dekker and Parker, 1994). The isozymes differ in substrate and activator preferences and fulfill distinct physiological roles (Kikkawa et al., 1989). All of the PKC isozymes have in common a physiological requirement for activation by the lipophilic second messenger diacylglycerol (DAG), with the exceptions of ζ and ι. PKC is the major cellular receptor for the tumor-promoting phorbol esters, which activate PKC in a manner very similar to DAG (Kikkawa et al., 1989; Bell and Burns, 1991; Newton, 1993). The use of the potent and selective phorbol esters as PKC activators has contributed to making the PKCs among the most thoroughly studied families of protein kinases in cellular signaling.

PKC activation is thought to proceed via the removal of an N-terminal autoinhibitory domain from the catalytic site (Orr and Newton, 1994; Kemp et al., 1994), but detailed structural information on the process of binding and activation of PKCs by DAG and tumor promoters has been scant. Both DAG and phorbol ester binding occur at two conserved cysteine-rich regions of PKC (Ono et al., 1989; Burns and Bell, 1991; Quest et al., 1994; Kazanietz et al., 1994). The first and second cysteine-rich regions are closely related and are referred to as the cys1 and cys2 domains, respectively. Both regions together are referred to as the C1 domain. Each of the cys1 and cys2 domains binds two zinc ions (Ahmed et al., 1991; Hubbard et al., 1991). The solution structure of the cys2 domain of PKCα determined in the absence of activators (Hommel et al., 1994) shows that the domain contains two small β sheets and that the two zinc-binding sites are formed by noncontiguous sections of primary sequence. Although these domains are sometimes referred to as zinc fingers, they are structurally unrelated to any of the nucleic acid–binding zinc finger proteins. Recombinant PKC cys1 and cys2 domains bind to phorbol esters and DAG with essentially the same high affinities as do intact PKCs (Ono et al., 1989; Burns and Bell, 1991; Quest et al., 1994; Kazanietz et al., 1994). These domains also bind several other classes of pharmacologically active natural products, including the potent PKC-directed anticancer agent bryostatin-1 (Pettit, 1991).

Despite intense interest in the structure and mechanism of PKC, intact PKCs have so far resisted experimental structure determination. The phorbol ester–activated form of PKC is particularly recalcitrant because it becomes tightly associated with the membrane fraction and is highly flexible as judged by proteolytic susceptibility (Burns and Bell, 1991; Lester, 1992; Newton, 1993). Both of these factors are highly unfavorable for structural studies. As part of an alternative "piecemeal" approach to understanding the active form of PKC, we have determined the crystal structure of a single cysteine-rich activator-binding domain both alone and in complex with the agonist phorbol 13-acetate. The complex structure has been refined to an R factor of 19.4% at 2.2 Å resolution, which allows an accurate analysis of the intricate hydrogen-bonding network in the activator-binding site.

Results and Discussion

Structure and Conformation of the Cys2 Domain

The cys2 domain of PKCδ (Figure 1) consists of two small β sheets and a short C-terminal α helix. Phorbol binds between residues 239–242 and 251–254 (Figures 1–2), which are in or near the β conformation and comprise most of β2 and β3. Except for one hydrogen bond between 242 and 251, these sections do not form direct β sheet hydrogen bonds. The four rings of phorbol are inserted lengthwise into a narrow groove between the two segments, with the C20 alcohol buried in the bottom. The bottom of the groove is formed by the side chains of Tyr-238, Leu-251, and Gln-257. The walls are formed by the main chain from 239–242 and 250–254 and the side chains of Met-239, Pro-241, Thr-242, Leu-250, and Leu-254.

In the absence of phorbol binding, the gap between the strands contains bound water molecules that form bridging hydrogen bonds like those at the ends of β sheets in other proteins (Finer-Moore et al., 1992). Bound phorbol displaces these water molecules, and the C3, C4, and C20
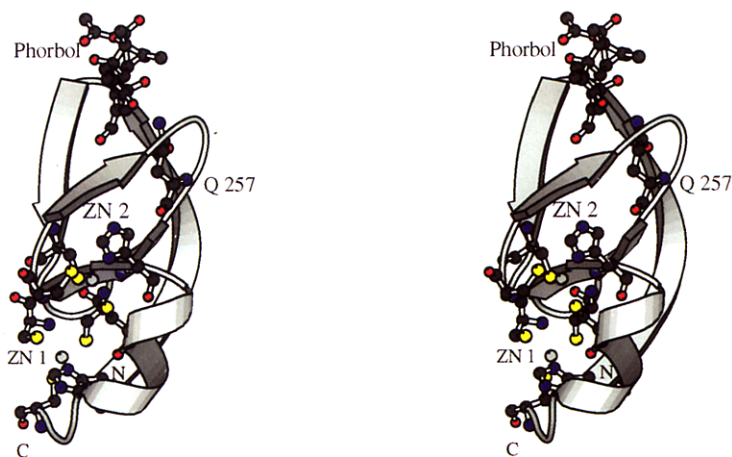
Figure 1. Stereoview of Phorbol Ester Binding to the Cys2 Domain

Stereoview drawn with Molscript (Kraulis, 1991).

oxygens replace the lost bridging hydrogen bonds. The PKC activator-binding site is thus constructed by pulling apart two β strands to generate unpaired hydrogen-bonding partners for the ligand. To our knowledge, the "unzipped" β sheet of the PKC activator-binding domains provides an unprecedented architecture for a small molecule-binding site.

The overall protein fold in the crystal structure is in reasonably close agreement with the solution structure (Hommel et al., 1994). The main-chain backbone differs by 1.8 Å rms for all residues. The largest differences, up to 7 Å, are concentrated near β2 and β3 and at the C-terminus, which are not well defined in the solution structure. The well-defined structure of the two phorbol-binding segments of β2 and β3 in the crystal structure is in contrast with the lack of definition of these regions in the solution structure (Hommel et al., 1994). These segments are well ordered (<B> = 15 Å²) in the crystal both in the presence and absence of phorbol. In solution, residues of the cys2 domain of PKCα corresponding to 239–240 and 254–257 of PKCδ are not well defined by experiment. The absence of bound phorbol in the solution structure cannot account for the apparent difference, because the crystal structure is equally rigid regardless of phorbol binding.

The apparent discrepancy could be explained if these regions were highly mobile in solution but not in the crystal, or if there were simply not enough nuclear Overhauser

effect (NOE) constraints to define these regions. Crystal contacts bury 45% of the total solvent-accessible surface area (Lee and Richards, 1971) of the protein; 59% of this buried surface area involves hydrophobic interactions. Tyr-238, Met-239, Phe-243, and Trp-252, which are adjacent in sequence to the phorbol-binding residues, are almost entirely buried in hydrophobic crystal contacts. These extensive hydrophobic contacts might be responsible for anchoring and rigidifying the phorbol-binding segments relative to the solution state. If this is the case, it is intriguing that the conformation stabilized by the crystal contacts is one capable of binding phorbol. Alternatively, β2 and β3 might be rigid even in solution. Most of the phorbol-binding segments of β2 and β3 are about 3 Å farther apart than if they had been in a conventional β sheet. Furthermore, most of the side chains in these regions have few interactions with the rest of the protein. Water-mediated, rather than direct, interactions play a major role in stabilizing the local structure in the unliganded state. Under these conditions, it would not be surprising if relatively few NOEs were to exist.

Structural Determinants for Phorbol Ester Binding

Five hydrogen bonds are formed between three of the phorbol oxygens and the protein (Figure 3). The C3 oxygen accepts a hydrogen bond from the main-chain amide of Gly-253. The C4 hydroxyl donates a hydrogen bond to the
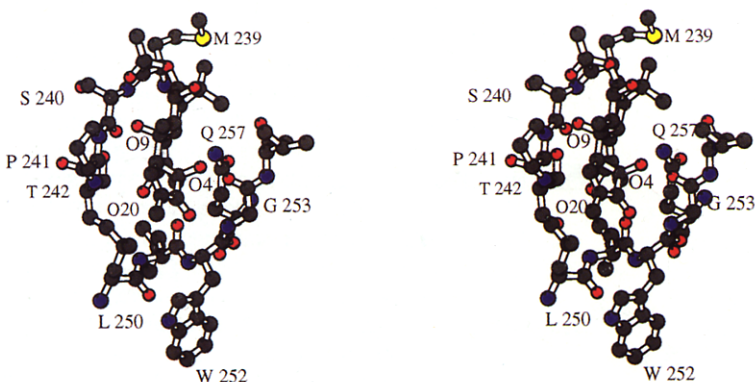

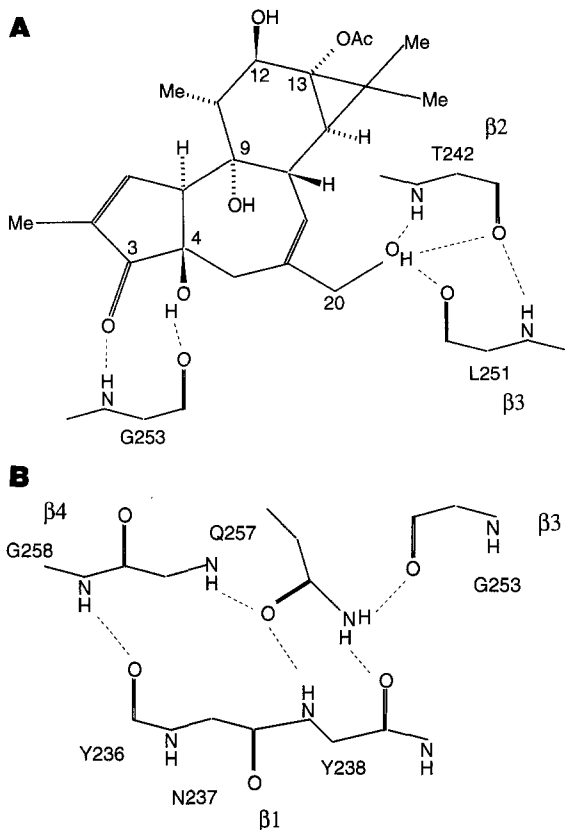Figure 2. Stereoview of the Phorbol Ester-Binding Site

A

B

Figure 3. Hydrogen Bond Networks at the Phorbol Ester–Binding Site

(A) Schematic of hydrogen-bonding interactions in the phorbol-binding site.

(B) Schematic of the role of the consensus Gln-257 at the junction between the large β sheet and the pulled-apart portion of the small β sheet. Secondary structure elements are identified for residues shown. Gly-253 immediately follows the end of β3.
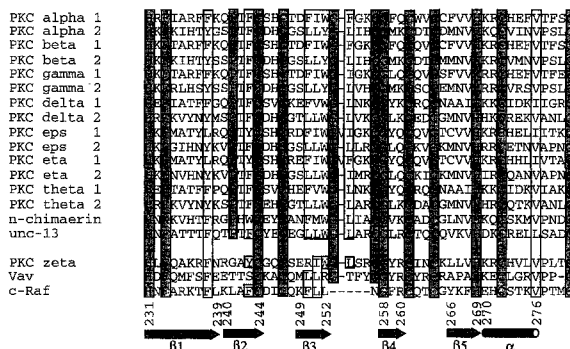

Figure 4. Alignment of PKC Cysteine-Rich Domains

Proteins in the upper group bind phorbol esters and those in the lower group do not. Identically conserved residues are enclosed in stippled boxes. Conserved but nonidentical residues implicated by the structure in binding or structural integrity of the domain are shown in open boxes. Secondary structure elements and PKCδ cys2 numbering are shown below the sequences. The sequence of PKCα is from bovine; PKCβ, PKCγ, PKCδ, and PKCε are from rat; PKCη, PKCθ, PKCζ, and Vav are from murine; n-chimaerin and c-Raf are from human; and unc-13 is from C. elegans. Domains of PKCs containing both cys1 and cys2 are labeled (1) and (2). PKC homologs whose phorbol ester–binding properties are unknown are not shown. Details of the alignment are described by Kazanietz et al. (1994).

main-chain carbonyl of Gly-253. The C20 hydroxyl accepts a hydrogen bond from the main-chain amide of Thr-242 and donates a bifurcated hydrogen bond to the main-chain carbonyls of Thr-242 and Leu-251, acting as an interstrand bridge. The C12 hydroxyl faces outward from the binding site. Neither the C9 hydroxyl nor the 13-acetyl hydrogen bond with the protein, but form an intramolecular hydrogen bond instead. Since both of the normal positions of esterification point away from the protein, the tails of long-chain phorbol esters probably do not interact directly with the protein. The three-, five-, and seven-membered phorbol rings and the 13-acetyl group have numerous van der Waals interactions with both the polar bottom and the hydrophobic sides of the groove. The six-membered ring has no interactions except for a single contact between the bottom of the ring and the main chain at Met-239. This latter portion of the phorbol is relatively mobile. B factors for this portion of the phorbol are in the 30–41 Å² range compared with 16 Å² for the most tightly bound phorbol atom, O20.

Binding leads to a 0.4 Å opening of the groove as measured between the main chain of Pro-241 and Gly-253. This shift is only marginally greater than the estimated coordinate error, but appears to be required to prevent a

steric conflict between the C4 oxygen and the main-chain carbonyl at Gly-253. The 0.3 Å rms overall main-chain atomic coordinate difference between the entire unliganded and phorbol-bound structures is probably insignificant.

Structure–activity relationships of phorbol esters and other PKC activators have been under intense study for more than 20 years (Hecker, 1978; Rando and Kishi, 1992). The complex structure explains much of the observed structure–activity data. 4-deoxy phorbol esters, which are active but have diminished affinity (Hecker, 1978), cannot form a hydrogen bond with the main-chain carbonyl at Gly-253. Methylation of the C4 oxygen would destroy its ability to donate a hydrogen bond to the Gly-253 carbonyl and create a severe steric conflict, explaining the inactivity of 4-O-methyl phorbol esters (Hecker, 1978). The lack of interactions involving the C12 hydroxyl explains the high affinity of 12-deoxyphorbol esters (Hecker, 1978). The O9 hydroxyl and acetyl carbonyl may be important because removal of either one of these polar moieties separately would leave the other with an unsatisfied hydrogen bond in the lipid phase. Phorbol esters and DAG bind competitively through interactions that have long been believed to be stereochemically equivalent (Rando and Kishi, 1992). The tightly packed surroundings of the C20 hydroxyl and its role in both donating and accepting hydrogen bonds are consistent with the model-based prediction (Rando and Kishi, 1992) that this position is analogous to the 3-hydroxyl of DAG. Local packing is consistent with differences in activity between diastereomers of 3-methyl DAG (Rando and Kishi, 1992).

Implications for PKC Homology Domains of raf and vav Proto-Oncogenes

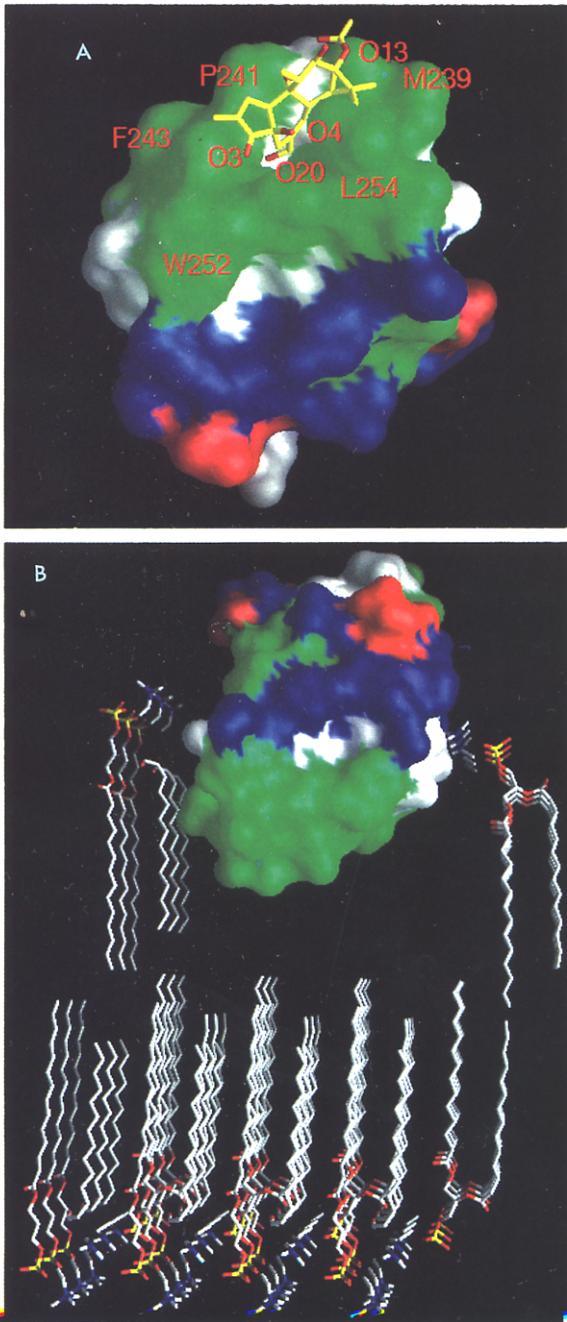One copy of the PKC cysteine-rich domain is present in

Figure 5. Molecular Surface Properties of the Cys2 Domain

(A) Molecular surface of the cys2 domain colored by residue type (A. Nicholls, GRASP, Columbia University). Phorbol binds in the deep groove at the top of the structure, shown with carbons colored yellow and oxygens colored red. On the protein surface, hydrophobic residues are green, positively charged residues are blue, negatively charged residues are red, and neutral polar residues are white.

(B) Model for the membrane-inserted form of the cys2–phorbol ester complex based on the molecular surface of the protein–phorbol complex and the crystal structure of dimyristoyl phosphorylcholine (Pascher and Pearson, 1979; Hauser et al., 1981). The molecular surface of the protein–phorbol complex is colored as above, except that phorbol is also colored green. The membrane model is intended only to represent the estimated depth of penetration of the protein into the bilayer. Lipids in front and in back of the domain have been removed for clarity, and no effort has been made to model the membrane structure immediately below the domain.

several other signaling proteins, including the nonphorbol ester–binding proto-oncogene proteins Vav and c-Raf (Figure 4). Vav, c-Raf, and the nonphorbol ester–binding isozyme PKCζ, all diverge from the phorbol ester–binding PKC consensus sequence at the position corresponding to Pro-241 (Kazanietz et al., 1994). The nonphorbol ester–binding proteins differ at other positions, but have no other common points of divergence. The restriction of the ϕ angle of Pro to $-60°$ prevents an antiparallel arrangement of the adjoining peptide planes, helping to prevent residues 240–242 from "zipping-up" with 251–253 into a β sheet.

The complex shows how two other PKC consensus residues help form the phorbol-binding site. Gly-253 is a key phorbol ligand and occupies angles (ϕ, ψ) that are disallowed for other residues. The Gln-257 side chain does not interact with phorbol, but forms bridging hydrogen bonds where the large β sheet comes apart at one end of the binding groove (Figure 3). The absolute conservation of the consensus Pro and Gln suggests that destabilization of hydrogen bonding between the two separated strands is critical for activator binding.

Restoring the consensus sequence to PKCζ by mutagenesis fails to confer phorbol binding (Kazanietz et al., 1994); hence, nonidentical residues are also required. Ser-240 is predicted to be within the membrane. This position is neutral in phorbol-binding proteins, but charged in some of the nonphorbol-binding proteins. In phorbol-binding proteins, the position corresponding to Ser-240 can be either Ser, Gln, Gly, or Val, making it the most variable binding site residue and suggesting a role in isozymic differences in activator specificity. Phe-243, Leu-250, Trp-252, and Leu-254 are all exposed and positioned to point into the membrane. These four positions are hydrophobic in all phorbol-binding proteins, but sometimes polar in nonphorbol-binding proteins. Tyr-238 and Leu-251 are mostly buried and form part of the floor of the binding groove; they correspond to hydrophobic residues in all sequences.

Structural Basis for Phorbol Ester–Promoted Membrane Insertion

The structure shows how membrane insertion (Lester, 1992) by PKCs might occur. The "top" third of the surface (Figure 5) is composed almost entirely of hydrophobic residues and is completely devoid of charged groups. Soluble proteins almost never contain a contiguous hydrophobic region covering such a large proportion of the entire surface. The "middle" third is overwhelmingly composed of positively charged side chains. The chain termini are close together at the "bottom" of the domain, suggesting connections to soluble domains will be well above the membrane. The layered surface suggests the cys2 domain could bury itself top down 6–8 Å into the bilayer (Figure 5). Similar mechanisms for membrane insertion are thought to occur for defensins (Hill et al., 1991) and prostaglandin H_2 synthase (Picot et al., 1994). Some of the basic side chains from the middle of the domain are positioned to interact with acidic phospholipid headgroups.

PKC activator domain partitioning into the membrane is strongly favored by the presence of phorbol or DAG

Table 1. Data Reduction and Phasing Statistics as a Function of Resolution

Data Reduction									
d_{min} (Å)	All	3.76	2.98	2.61	2.37	2.20	2.07	1.95	
R_{merge} (MAD λ2)	0.072	0.061	0.069	0.082	0.095	0.106			
R_{merge} (lab)	0.061	0.045	0.065	0.089	0.105	0.113	0.110	0.098	
R_{merge} (phorbol)	0.067	0.046	0.068	0.101	0.138	0.161			
Complete (MAD)	79.6	76.6	80.5	79.8	81.6	80.2			
Complete (lab)	88.8	100.0	100.0	100.0	96.3	82.3	67.4	44.0	
Complete (phorbol)	94.6	99.3	98.9	98.2	96.7	79.4			
Refinement									
R_{cryst} (unbound)	0.197	0.165	0.180	0.205	0.216	0.237	0.231	0.262	
R_{cryst} (phorbol)	0.194	0.159	0.186	0.214	0.236	0.252			
MAD Phasing									
d_{min} (Å)	All	9.4	6.2	4.9	4.2	3.7	3.4	3.1	2.8
N	1242	68	91	136	151	176	189	220	211
R_{Cullis}	0.48	0.37	0.33	0.38	0.59	0.53	0.66	0.58	0.44
F_H/E_{rms} (iso)	1.72	1.63	1.84	1.93	1.72	1.57	1.36	1.90	2.20
F_H/E_{rms} (ano)	1.87	0.94	1.02	1.00	2.53	3.11	3.20	1.56	1.63
Figure of merit	0.54	0.49	0.52	0.53	0.57	0.54	0.47	0.53	0.63

$R_{merge} = \Sigma|I_i - <I>|/\Sigma <I>$, with Bijvoet pairs treated as equivalent. R_{merge} values for MAD data sets were very similar for all three wavelengths and are shown for the wavelength at which they were largest. "Complete" is the percentage of possible reflections measured with $I/\sigma(I) \geqslant 0$ ($I/\sigma(I) \geqslant 1$ for MAD data); $R_{cryst} = \Sigma|F_o - F_c|/\Sigma F_o$ for all amplitudes (no $F/\sigma(F)$ cut-off applied) measured in the indicated resolution bin; N is the number of reflections for which MAD phases were calculated; $R_{Cullis} = \Sigma||F_{PH} \pm F_P| - F_H|/\Sigma|F_{PH} \pm F_P|$ for the mock isomorphous differences of centric reflections due to dispersive differences; $<F_H>/E_{rms}$ (iso) and (ano) indicate dispersive and anomalous phasing power for acentric reflections. For data reduction and phasing statistics, "All" refers to all data to the highest resolution used. For R_{cryst}, "All" refers to data from 6.0 Å to the highest resolution used. Columns show statistics for bins of data with the upper resolution limit indicated. The lower resolution limit for each bin is that of the preceding bin; for the leftmost bin, it is the same as the overall limit.

(Burns and Bell, 1991; Lester, 1992; Newton, 1993). This behavior can be explained by the structure of the activator-binding site and by the nature of the protein surface. Membrane insertion of the unliganded activator-binding site would have to lead to either a loss of hydration between the unzipped strands or to the insertion of bound water molecules into the membrane along with the protein. Either of these situations involve several unsatisfied hydrogen bonds at the protein–membrane interface, which is highly unfavorable. By contrast, phorbol binding satisfies the hydrogen bonding potential of the activator-binding groove. The activator forms a hydrophobic cap over the exposed polar main-chain groups. When an activator is bound, the domain can fully bury its hydrophobic exterior surface in the membrane without suffering an unfavorable loss of hydrogen bonds in the groove.

Water-soluble short-chain phorbol esters such as phorbol 13-acetate can function as PKC activators, but with potency reduced by several orders of magnitude (M. G. K. and P. M. B., unpublished data). Only the water-insoluble long-chain phorbol esters are potent PKC activators. Because these compounds are completely partitioned into the membrane, protein–phorbol binding is directly linked to membrane association by the protein. In combination, these factors can reasonably account for the coupling of ligand binding to membrane insertion.

The Role of Phorbol Ester Binding in PKC Activation

The structure of the activator-binding domain–phorbol ester complex helps clarify the role of phorbol esters in PKC activation. Phorbol ester binding does not produce a signif-

icant conformational change within the activator-binding domain. Rather, it acts to cover the polar interior of the groove and completes a contiguous hydrophobic surface over a large portion of the domain. The long-chain lipid tails of PKC activators are probably not directly involved in binding to PKC, but instead retain the activator within the membrane. The retention of the long-chain phorbol esters in the membrane means that the favorable free energy of protein–phorbol binding can be used to drive the insertion of the protein into the membrane. The present structural results suggest that phorbol esters activate PKC by altering the nature of the protein surface and by stabilizing the membrane-inserted state, rather than by inducing a conformational change at the activator-binding site.

Experimental Procedures

Protein Expression and Purification

DNA coding for residues 231–280 of mouse PKCδ (Mischak et al., 1991) was subcloned into the BamHI and EcoRI sites of pGEX-2T (Pharmacia) and expressed as a thrombin-cleavable glutathione S-transferase fusion protein in Escherichia coli XL1-Blue. Phorbol ester binding was confirmed as described (Kazanietz et al., 1994). The vector construction led to a postcleavage expressed protein containing N- and C-terminal extensions with the sequences Gly-Ser-Arg-Arg-Ala-Ser-Val-Gly-Ser and Glu-Phe-Ile-Val-Thr-Asp, respectively; hence, the entire protein contains 65 amino acid residues. Cells were grown in an 8 liter fermenter (BioFlo IV, New Brunswick Scientific) to an optical density at 600 nm of 10.0, induced with 0.3 mM IPTG, and harvested 6 hr after induction. Cells were lysed in 1 liter of phosphate-buffered saline (PBS), 1 mg/ml lysozyme, 1% Triton X-100, 1 μg/ml leupeptin, 1 mM PMSF. The suspension was sonicated and centrifuged at 30,000 × g for 30 min. Glutathione–Sepharose 4B beads (20 ml) (Pharmacia) were added to the supernatant. The resin was equilibrated and washed according to the instructions of the manufacturer. Cleavage
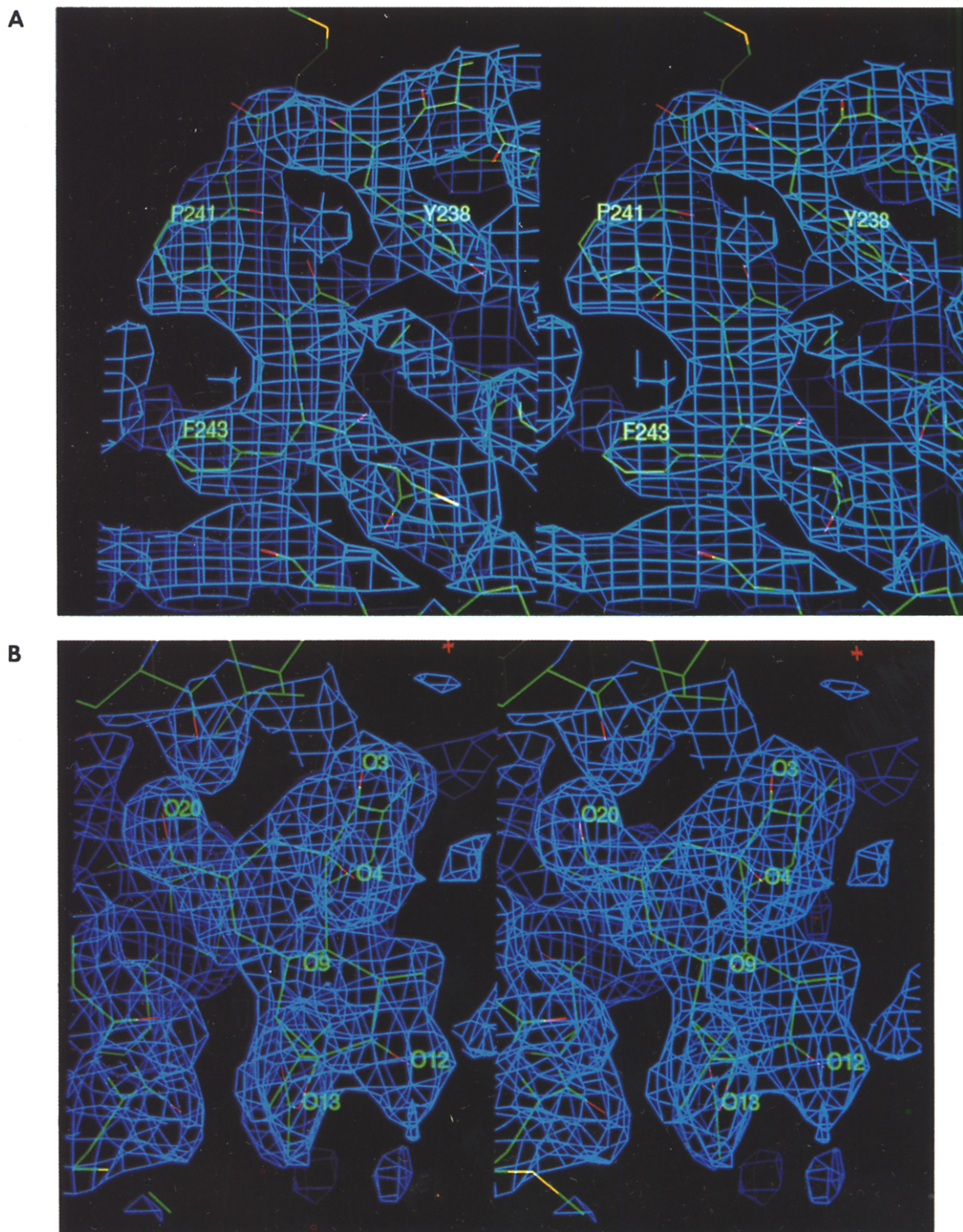
A

B

Figure 6. Electron Density at the Phorbol Ester–Binding Site

(A) Refined structure of the cys2 domain superimposed on 2.8 Å solvent-flattened MAD density (1.0 σ).

(B) Phorbol complex superimposed on 2.2 Å $[2F_o - F_c]\alpha_{calc}$ density (0.6 σ). The appearance of the map is similar if contoured at 1.0 σ, except that the off-ring methyl of the six-membered ring, which has a high B factor and no interactions with the protein, is out of density.

from the resin was carried out with 20 U of thrombin (Boehringer-Mannheim) in 20 ml of PBS for 16 hr at 4°C. The cleaved protein was collected from the supernatant and centrifuged for 30 min at 30,000 × g. The supernatant was loaded (10 ml at a time) on a 2.6 × 60 cm Superdex S-200 gel filtration column (Pharmacia) equilibrated in 0.5 M NaCl, 0.1 M triethanolamine HCl (pH 7.0) and run at 1 ml/min. Peak fractions were pooled, adjusted to 10% glycerol, 1 mM PMSF, 1 mM DTT, and stored at −80°C.

Protein Crystallization

Protein was concentrated to 8 mg/ml by precipitation with 55% ammonium sulfate and resuspension in 0.1 M phosphate buffer (pH 6.8), 1 mM DTT. Microcrystals were obtained by hanging drop vapor diffusion, using a sparse matrix screen (Hampton Research) to obtain initial conditions. Protein (6 μl) was mixed with an equal volume of well solution containing 25% isopropanol, 0.2 M ammonium acetate, 0.1 M sodium phosphate (pH 6.8) and incubated at 4°C. Using the micro-

Table 2. MAD Parameters

	<ΔF'>/<F>		<ΔF">/<F>	f'	f"
	λ₁	λ₂			
λ₁	—	—	0.031	−9.19	2.04
λ₂	0.050	—	0.051	−7.11	4.26
λ₃	0.085	0.069	0.049	−3.53	3.79

ΔF' and ΔF" are the measured dispersive and anomalous amplitude differences, f' and f" are in electrons, and the wavelengths used are λ₁ = 1.2826, λ₂ = 1.2818, and λ₃ = 1.2616 Å.

Table 3. Parameters of the Refined Models

Parameter	Free	Complex
d_{min} (Å)	1.95	2.20
N (6.0–d_{min})	4073	3215
R (6.0–d_{min})	0.197	0.194
R (40.0–d_{min})	0.224	0.212
Rms Δbond (Å)	0.014	0.014
Rms Δangle (degrees)	2.9	3.2
Rms ΔB (bonds)	3.3	3.2
Number of protein atoms	510	489
Protein <B> (Å²)	16.3	19.4
Protein B_{min} (Å²)	2.0	2.0
Protein B_{max} (Å²)	58.6	59.0
Number of phorbol atoms	0	29
Phorbol <B> (Å²)	—	34.3
Phorbol B_{min} (Å²)	—	16.0
Phorbol B_{max} (Å²)	—	41.0
Number of water molecules	59	39
Water <B> (Å²)	31.5	29.9
Water B_{min} (Å²)	4.5	7.0
Water B_{max} (Å²)	49.0	48.0

N is the number of reflections used in refinement, R is the crystallographic R factor defined in Table 1, and B refers to refined atomic thermal parameters. All quantities are obtained from XPLOR (Brünger et al., 1987) except the R factor from 40.0 Å to d_{min} that was obtained using TNT (Tronrud et al., 1987) with four-parameter scaling and the correlated B factor deviations of bonded atoms that were calculated with the BCORREL module of TNT (Tronrud et al., 1987).

crystals as seeds, plates of approximately 0.4 mm × 0.4 mm × 0.01 mm were obtained. Cocrystallization with phorbol 13-acetate was carried out as above, except with the addition of 1 mM phorbol 13-acetate (LC Laboratories) and 5% methanol, and yielded crystals no larger than 0.3 mm × 0.3 mm × 0.01 mm.

Crystallographic Data Collection

Data were collected from frozen crystals using graphite-monochromated Cu Kα radiation from a Rigaku RU-200 rotating anode source operating at 5 kW and an RAXIS II imaging plate detector system (Table 1). Crystals were equilibrated in 15% sucrose, 25% PEG 4000, 0.1 M sodium phosphate buffer (pH 7.2) and mounted in rayon loops prior to flash freezing in a dry nitrogen stream at −180°C. Data were collected in 2° exposures for 40 min per exposure. The space group and cell dimensions are C222₁ and a = 32.4 Å, b = 63.5 Å, c = 65.5 Å (Table 1), based on autoindexing with DENZO (Z. Otwinowski, Department of Molecular Biophysics and Biochemistry, Yale University) and manual inspection of systematic absences. Multiwavelength anomalous dispersion (MAD) data were collected from frozen crystals at the X4A beamline, National Synchrotron Light Source, Brookhaven National Laboratory, at three wavelengths (Table 2). Bijvoet pairs were collected using inverse beam geometry. Image plates were exposed for 4° oscillations with a 1° overlap, for 60–90 s each, and scanned on a Fuji BAS 2000 scanner. Data integration and reduction were carried out with DENZO, and only fully measured reflections were retained.

MAD Structure Determination and Refinement

Bijvoet and wavelength scaling was carried out by local scaling using an unpublished program written by J. H. H. Anomalous scattering factors for native zinc ions (Table 2) were obtained from a fluorescence scan of the crystal (Hendrickson et al., 1988). Native zinc structure factors were estimated (Terwilliger, 1994a) and used to locate the zinc ions in a Patterson synthesis. Dispersive and anomalous differences were cast into isomorphous replacement formalism and refined with HEAVY (Terwilliger, 1994b) using the origin-removed Patterson method (Table 1). The resulting 2.8 Å resolution map was subjected to solvent flattening (Wang, 1985) in reciprocal space (W. Furey, PHASES, University of of Pittsburgh) with a solvent fraction of 0.45 (Figure 6). Map interpretation with CHAIN (Sack, 1988) was initiated at the zinc sites and facilitated by the availability of the solution structure of the homologous cys2 domain of PKCα. The structure was refined with XPLOR (Brünger et al., 1987) by slow cooling from 6000 K to 300 K, followed by conjugate gradients minimization and restrained temperature factor refinement versus all measured amplitudes (no F/σ(F) cutoff was applied and no "test set" was excluded from refinement) from 6.0 to 1.95 Å data (Table 3). The refined model of the unliganded domain includes the entire activator-binding domain and all of the vector-derived sequences except for the first residue in the N-terminal extension and the last residue in the C-terminal extension (Table 3). The overall R factor is 0.197 for all data in the resolution range 6.0 to 1.95 Å (Table 3).

Phorbol 13-acetate was located using [F$_{obs}$(phorbol) − F$_{obs}$(native)]α$_{MAD}$, [F$_{obs}$(phorbol) − F$_{obs}$(native)]α$_{calc}$, and [F$_{obs}$(phorbol) − F$_{calc}$(omit)]α$_{calc}$ difference syntheses. All maps used in refinement were calculated with all low resolution data included, using four-parameter scaling carried out with TNT (Tronrud et al., 1987) to account for the scattering contribution of bulk solvent. The structure of the phorbol complex was refined as above, except using all measured amplitudes from 6.0 to 2.2

Å (Table 3). Side chains of Arg-273, Glu-274, and the first vector-derived Arg were omitted from the complex model because of their high mobility. There are no nonglycine (φ, ψ) pairs in the disallowed region of the Ramachandran plot of either model, and all stereochemical parameters are as good or better than expected for the resolution of the refinements (Laskowski et al., 1993). The overall R factor for the phorbol complex model is 0.194 for all data from 6.0 to 2.20 Å (Tables 1 and 3). Coordinates will be deposited with the Protein Data Bank at Brookhaven and can be obtained prior to release by sending e-mail to HURLEY@TOVE.NIDDK.NIH.GOV.

References

Ahmed, S., Kozma, R., Lee, J., Monfries, C., Harden, N., and Lim, L. (1991). The cysteine-rich domain of human proteins, neuronal chimaerin, protein kinase C and diacylglycerol kinase binds zinc. Biochem. J. 280, 233–241.

Bell, R. M., and Burns, D. J. (1991). Lipid activation of protein kinase C. J. Biol. Chem. 266, 4661–4664.

Brünger, A. T., Kuriyan, J., and Karplus, M. (1987). Crystallographic R-factor refinement by molecular dynamics. Science 235, 458–460.

Burns, D. J., and Bell, R. M. (1991). Protein kinase C contains two phorbol ester binding domains. J. Biol. Chem. 266, 18330–18338.

Dekker, L. V., and Parker, P. J. (1994). Protein kinase C: a question of specificity. Trends Biochem. Sci. 19, 73–77.

Finer-Moore, J. S., Kossiakoff, A. A., Hurley, J. H., Earnest, T. N., and Stroud, R. M. (1992). Solvent structure in crystals of trypsin determined by X-ray and neutron diffraction. Proteins 12, 203–222.

Hauser, H., Pascher, I., Pearson, R. H., and Sundell, S. (1981). Preferred conformation and molecular packing of phosphatidylethanolamine and phosphatidylcholine. Biochim. Biophys. Acta 650, 21–51.

Hecker, E. (1978). Structure–activity relationships in diterpene esters irritant and cocarcinogenic to mouse skin. In Carcinogenesis: A Comprehensive Survey, Mechanisms of Tumor Promotion and Cocarcinogenesis, Volume 2, T. J. Slaga, A. Sivak, and R. K. Boutwell, eds. (New York: Raven), pp. 11–48.

Hendrickson, W. A., Smith, J. L., Phizackerley, R. P., and Merritt, E. A. (1988). Crystallographic structure analysis of lamprey hemoglobin from anomalous dispersion of synchrotron radiation. Proteins 4, 77–88.

Hill, C. P., Yee, J., Selsted, M. E., and Eisenberg, D. E. (1991). Crystal structure of defensin HNP-3, an amphiphilic dimer: mechanisms of membrane permeabilization. Science 251, 1481–1485.

Hommel, U., Zurini, M., and Luyten, M. (1994). Solution structure of a cysteine rich domain of rat protein kinase C. Nature Struct. Biol. 1, 383–387.

Hubbard, S. R., Bishop, W. R., Kirschmeier, P., George, S. J., Cramer, S. P., and Hendrickson, W. A. (1991). Identification and characterization of zinc binding sites in protein kinase C. Science 254, 1776–1778.

Kazanietz, M. G., Bustelo, X. R., Barbacid, M., Kolch, W., Mischak, H., Wong, G., Pettit, G. R., Bruns, J. D., and Blumberg, P. M. (1994). Zinc finger domains and phorbol ester pharmacophore: analysis of binding to mutated form of protein kinase Cζ and the vav and c-raf proto-oncogene products. J. Biol. Chem. 269, 11590–11594.

Kemp, B. E., Parker, M. W., Hu, S., Tiganis, T., and House, C. (1994). Substrate and pseudosubstrate interactions with protein kinases: determinants of specificity. Trends Biochem. Sci. 19, 440–444.

Kikkawa, U., Kishimoto, A., and Nishizuka, Y. (1989). The protein kinase C family: heterogeneity and its implications. Annu. Rev. Biochem. 58, 31–44.

Kraulis, P. J. (1991). MOLSCRIPT: a program to produce both detailed and schematic plots of protein structures. J. Appl. Crystallogr. 24, 946–950.

Laskowski, R. A., MacArthur, M. W., Moss, D. S., and Thornton, J. M. (1993). PROCHECK: a program to check the stereochemical quality of protein structures. J. Appl. Crystallogr. 26, 283–291.

Lee, B., and Richards, F. M. (1971). The interpretation of protein structures: estimation of static accessibility. J. Mol. Biol. 55, 379–400.

Lester, D. S. (1992). Membrane-associated protein kinase C. In Protein Kinase C, Current Concepts and Future Perspectives, D. S. Lester and R. M. Epand, eds. (Chichester, England: Ellis Horwood), pp. 80–101.

Mischak, H., Bodenteich, A., Kolch, W., Goodnight, J., Hofer, F., and Mushinski, J. F. (1991). Mouse protein kinase C-δ, the major isoform expressed in mouse hemopoietic cells: sequence of the cDNA, expression patterns, and characterization of the protein. Biochemistry 30, 7925–7931.

Newton, A. C. (1993). Interactions of proteins with lipid headgroups: lessons from protein kinase C. Annu. Rev. Biophys. Biomol. Struct. 22, 1–25.

Ono, Y., Fujii, T., Igarashi, K., Takayoshi, K., Tanaka, C. Ushio, K., and Nishizuka, Y. (1989). Phorbol ester binding to protein kinase C requires a cysteine-rich zinc-finger-like sequence. Proc. Natl. Acad. Sci. USA 86, 4868–4871.

Orr, J. W., and Newton, A. C. (1994). Intrapeptide regulation of protein kinase C. J. Biol. Chem. 269, 8383–8387.

Pascher, I., and Pearson, R. H. (1979). The molecular structure of lecithin hydrates. Nature 281, 499–501.

Pettit, G. R. (1991). The bryostatins. Prog. Chem. Org. Nat. Prod. 57, 154–190.

Picot, D., Loll, P. J., and Garavito, M. (1994). The X-ray crystal structure of the membrane protein prostaglandin H₂ synthase-1. Nature 367, 243–249.

Quest, A. F. G., Bardes, E. S. G., and Bell, R. M. (1994). A phorbol ester binding domain of protein kinase Cγ: deletion analysis of the cys2 domain defines a minimal 43-amino acid peptide. J. Biol. Chem. 269, 2961–2970.

Rando, R. R., and Kishi, Y. (1992). The structural basis of protein kinase C activation by diacylglycerols and tumor promoters. In Protein Kinase C, Current Concepts and Future Perspectives, D. S. Lester and R. M. Epand, eds. (Chichester, England: Ellis Horwood), pp. 41–61.

Sack, J. S. (1988). CHAIN: a crystallographic modeling program. J. Mol. Graph. 6, 224–225.

Terwilliger, T. C. (1994a). MAD Phasing: Bayesian estimates of F_A. Acta Crystallogr. D50, 11–16.

Terwilliger, T. C. (1994b). MAD Phasing: treatment of dispersive differences as isomorphous replacement information. Acta Crystallogr. D50, 17–23.

Tronrud, D. E., Ten Eyck, L. F., and Matthews, B. W. (1987). An efficient general purpose least-squares refinement program for macromolecular structures. Acta Crystallogr. A43, 489–501.

Wang, B. C. (1985). Resolution of phase ambiguity in macromolecular crystallography. Meth. Enzymol. 115, 90–112.